

D.A.A./LANCETT

NAG-1-462

IN-34

63688
21P.

FINAL TECHNICAL REPORT

NASA GRANT NO. NAG-1-462

"NUMERICAL SIMULATION OF TRANSITIONAL FLOW"

SEDAT BIRINGEN, PROJECT DIRECTOR

(NASA-CR-180293) NUMERICAL SIMULATION OF
TRANSITIONAL FLOW Final Technical Report
(New Hampshire Univ.) 21 p Avail: NTIS HC
AC2/MF A01 CSCL 20D

N87-26279

Unclas

G3/34 0063688

A NUMERICAL STUDY OF
TRANSITION CONTROL BY PERIODIC SUCTION-BLOWING

by

Sedat Biringen

Abstract

The applicability of active control of transition by periodic suction-blowing is investigated via direct numerical simulations of the Navier-Stokes equations. The time-evolution of finite-amplitude disturbances in plane channel flow is compared in detail with and without control. The analysis indicates that, for relatively small three-dimensional amplitudes, a two-dimensional control effectively reduces disturbance growth rates even for linearly unstable Reynolds numbers. After the flow goes through secondary instability, three-dimensional control seems necessary to stabilize the flow. An investigation of the temperature field suggests that passive temperature contamination is operative to reflect the flow dynamics during transition.

1. Introduction

The development of methods for laminar flow control (LFC) is of great interest due to potential applications in drag reduction. The implementation of such techniques may prove effective to increase the propulsion efficiency of aircraft, ships and submarines, thereby improving their performance. In wall-bounded flows, the application of constant suction as a means of LFC has been studied extensively. Experiments indicate a significant drag-reudction potential of this technique in airfoil technology for relatively low disturbance amplitudes, i.e. before non-linear effects dominate the flow.¹ In this method, the evolving boundary layer is modified by suction through a porous wall, in-

creasing the velocity gradient near the boundary and creating a more stable flow. As an alternative to this technique, more direct methods of flow control have been devised in which wave cancellation is utilized.²⁻⁵ Further developments in this direction were instigated by the experiments of Liepmann and Nosenchuck⁶, who demonstrated the applicability of active control in water by surface heating. However, due to different conductive-diffusive properties, this method has been marginally feasible in air.⁷

As a method independent of the physical characteristics of the fluid, transition control by periodic suction-blowing was investigated by Biringen⁸ in a numerical study. It was shown that a single-pulse, two-dimensional control wave of suitable amplitude and phase results in considerable reduction of disturbance amplitudes in plane channel flow. More recently, Kleiser and Laurien⁹ numerically investigated the applicability of a similar technique in the presence of subharmonic instability in plane channel flow. Along similar lines, Zang and Hussaini¹⁰ developed a novel spectral method for the solution of the incompressible Navier-Stokes equations and applied three-dimensional control suppressing selected modes in plane channel flow as well as in the periodic boundary layer. The application of active wall forcing for flow stabilization was investigated by Metcalfe et al.¹¹ and Kuhn et al.¹² in the periodic boundary layer and in plane channel flow, respectively. The potential usefulness of transition control by wave superposition suggested by these numerical investigations was verified by the wind-tunnel experiments of Strykowski and Sreenivasan¹³ demonstrating that two-dimensional Tollmien-Schlichting waves can be effectively cancelled by anti-phased two-dimensional control waves.

Although these studies point to the inherent applicability of transition control by periodic suction-blowing in the presence of two- and three-dimensional periodic disturbances, the success of the method (even strictly from a theoretical perspective) depends on other factors as well. The applicability of the method to broadband disturbance spectra and, as pointed out by Thomas³, the fate

of the residual field after interaction with the control wave remain as important issues to be considered. In this work, these queries are addressed via direct numerical simulations of the three-dimensional, time-dependent incompressible Navier-Stokes equations in the periodic plane channel flow. Despite the limiting assumption of flow periodicity along the homogeneous directions, Navier-Stokes simulations are gaining acceptance as a necessary supplement to experimental investigations. Such studies are especially useful in studying the late transition process dominated by three-dimensional, nonlinear effects. Issues concerning the effect of large suction amplitudes and a comparison of the present method with constant suction are briefly discussed in section 3, wherein a non-intrusive means of determining the phase of the control wave is also suggested. Further, the effectiveness of tagging the velocity/vorticity field by temperature is briefly investigated. In connection with this issue, some results from the temperature field which is treated as a passive scalar are presented.

2. The Calculation Procedure

The calculation procedure uses the incompressible Navier-Stokes equations in primitive-variable, energy-conserving form along with the continuity equation. A semi-implicit, pseudo-spectral method¹⁴ is employed to numerically integrate the governing equations. The computer code is vectorized for the VPS32 vector processor at NASA/Langley Research Center. Details of the solution procedure are provided elsewhere.^{15,16} Initial conditions are prescribed according to

$$u(x) = U(x_2, 0, 0) + u_{2D}(x_2) e^{i\alpha x_1} + u_{3D}(x_2) e^{i\alpha x_1 + i\beta x_3} \quad (1)$$

where $U(x_2, 0, 0)$ is the parabolic mean flow, $u_{2D}(x_2)$ and $u_{3D}(x_2)$ are the two- and three-dimensional eigen-solutions of the Orr-Sommerfeld equation, respectively.

All the cases were run at $Re=7500$, corresponding to a linearly unstable Reynolds number for this flow; here, $Re = U_0 h / \nu$, where U_0 is the channel centerline velocity, h is the channel half-thickness and ν is kinematic viscosity. Note that these initial conditions are of the Benney-Lin type and will result in the Klebanoff type transition characterized by non-staggered peak-valley splitting of the disturbance velocity. The existence of subharmonic instability in plane channel flow as a new mechanism for transition is now well documented. Herbert¹⁷ has found that this type of instability will operate at low disturbance amplitudes, whereas at higher amplitudes the type of instability depends on the background disturbance. Since the present work is concerned with initial disturbance amplitudes as high as 3%, we have not included subharmonic instability in our study.

The solution procedure assumes the flow to be periodic along the streamwise, x_1 , and spanwise, x_3 , coordinates. The governing equations were numerically integrated in a computational box with $0 \leq x_1 \leq 2\pi/\alpha$, $-1 \leq x_2 \leq 1$ and $0 \leq x_3 \leq 2\pi/\beta$, where the wave numbers of the fundamental disturbances were set to $\alpha=1$ and $\beta=1$ for all the cases; these wavenumbers were found to be adequate to provide a path to flow instability. Because of the assumed periodicity of the computed flow field, the x_1 -direction in the computation is interchangeable with the t (time)-coordinate in the laboratory. Consequently the periodic suction-blowing boundary conditions operated at the channel walls for one time step will have the same effect as an infinitesimally thin suction-blowing slot in the spatially evolving laboratory flow. For mass conservation, flow periodicity requires $\langle u_2 \rangle =$ constant where $\langle u_2 \rangle$ is the plane-averaged velocity along x_2 , leading to equal-amplitude periodic boundary conditions at the walls. Since, in this work, the control wave is set 180° out of phase with u_2 at the channel center, flow symmetry also requires equal phase for the wall boundary conditions at $x_2 = \pm 1$.

The temperature field is calculated from the "passive-scalar" equation

$$\frac{\partial \theta}{\partial t} + \frac{\partial(\theta u_i)}{\partial x_i} = \frac{1}{Pe} \frac{\partial^2 \theta}{\partial x_j \partial x_j} \quad (2)$$

where θ is the initial bulk temperature minus the fluid temperature, normalized by the difference between the initial bulk temperature and the wall temperature; Pe is the Peclet number, $Pe=(RePr)$. In this work, the value of the Prandtl number was set to $Pr=0.7$, and constant surface heating was assumed. Note that, in this analysis, the velocity field is uncoupled from the temperature field so that the temperature equation can be solved independently. For this purpose, the same numerical method as the velocity field was incorporated; the complete analysis of the temperature solution will be reported elsewhere.

3. Results and Discussion

In this section, the results for the three test cases presented in this work are discussed; a more detailed account is available in Refs. 18 and 19. The discussion centers on the time-evolution of the important Fourier components of u_1 . The development of the flow-field variables via three-dimensional pictorial representations is also investigated. Such illustrations are especially important to depict primary and/or residual three-dimensionality in the flow field. All the calculations were run on a $32 \times 51 \times 32$ grid with time step $\Delta T=0.025$. A summary of initial conditions and control wave amplitudes for each case is provided in Table 1.

3.1 Case 1: Three-Dimensional Initial Conditions with Low Background Noise (Random Field)

The cases reported by Biringen⁸ are essentially equivalent to controlling transition at a very early stage in an environment with no background disturbances. Here, consideration is given to a more complicated situation which contains more realistic elements, e.g. three-dimensionality and background noise. For this

case, maximum amplitudes of the initial disturbance field were set to $(u'_1)_{2D}^{\max} = 0.03U_0$, $(u'_1)_{3D}^{\max} = 0.0025U_0$ (for each 3D wave) and $(u'_1)_{\text{RAN}}^{\max} = 0.0001U_0$, with $(u'_1)_{\text{RAN}}$ corresponding to a random field (generated by a random number generator) representative of background noise. The procedure outlined in Ref. 8 was utilized: no slip boundary conditions were used on u at the channel walls and the flow was allowed to develop for $0 < T < 20$, where T is time non-dimensionalized by h/U_0 and ΔT is the time step. The control wave was then imposed for one time step at $T=20$ and $T=30$ as a wave anti-phased with the 2D Fourier mode $u'_2(1,0)$ at the channel center, with corresponding peak amplitudes of $0.023 U_0$ and $0.005 U_0$. The drawback caused by these large amplitudes was offset by the short pulse-duration of the control wave. The temporal development of $(u'_1)_{\max}$ and its important 2D Fourier modes $(1,0)$, $(2,0)$, $(3,0)$, as well as the primary 3D mode $(0,1)$, are displayed in Fig. 1. The immediate benefits resulting from interference with the control wave are clear: growth rates of the 2D harmonics $(2,0)$ and $(3,0)$ are completely reversed, indicating energy cut-off up to high wave numbers. The amplitudes of $(u'_1)_{\max}$ and 2D primary mode $(1,0)$ still grow but remain much lower than the uncontrolled case, whereas the 3D primary mode $(0,1)$ is unaffected by the control wave.

In Fig. 2, the distributions of $(u'_1)_{\text{RMS}}$ at $T=40$ reveal that the maximum intensity amplitude remains considerably lower for the controlled flow. The reduction in the intensity amplitude, $(u'_1)_{\text{RMS}}^{\max}$, is an indication of the diminished ability of the disturbance field to extract energy from the mean flow. Also in this Figure, the latent but significant effect of the background disturbance on the flow development is indicated by the cusp-like distributions of $(u'_1)_{\text{RMS}}$ around the channel center. Note that for both cases, i.e. with and without control, strong viscous effects attenuate the random field in the near-wall region, but close to the channel center and at later times the background noise begins to amplify. Although interference with 2D control efficiently reduces

intensity amplitudes in the wall region, its effects seem negligible on the random field containing a significant amount of energy in the three-dimensional modes. The outcome of the random field is investigated in greater detail in Fig. 3, where plots of $(u_1')_{\text{RMS}}^{\text{max}}$ over two periods along x_3 at $T=40$ are presented. For the uncontrolled case, the sinusoidal initial peak-valley splitting is retained, whereas for the controlled case the significant reduction in peak amplitude is accompanied by wave-front distortions, resulting in maxima occurring at the valleys and suggesting an increase in the number of spanwise vortex structures. This is a surprising result suggesting a potential for "explosive" growth provoked by the coupling of background noise on the residual field. This effect is further illustrated in Fig. 4, where three-dimensional iso-surfaces of streamwise vorticity, $\omega_x=0.10$, at $T=40$ are shown. A comparison of Figs. 4a and 4b unequivocally demonstrates that, while the elongated streamwise structures close to the wall are reduced in size, the control wave has no perceptible attenuating effect on flow three-dimensionality prevailing outside the wall region and caused by the initial random field.

3.2 Case 2: Three-Dimensional Initial Conditions With High Background Noise

The potential explosiveness of low-amplitude initial background noise was indicated in the preceding discussion. As an expansion on this idea, a situation is investigated in case 2 in which the initial amplitude of the background noise is increased to $(u_1')_{\text{RAN}}^{\text{max}} = 0.005 U_0$. In this case, the 2D control-pulse was applied at $T=20$ with a peak amplitude equal to $0.034 U_0$. The temporal development of the significant Fourier modes for the controlled flow is shown in Fig. 5. In accordance with the previous cases, the control wave leads to decaying 2D modes (1,0) and (2,0) with no significant change in the 3D mode (0,1). The most

striking aspect of this case is the sudden onset of an explosive instability leading to chaotic motion and an order of magnitude increase in the maximum disturbance amplitude. Since the one-dimensional energy spectrum still indicates energy concentration in the (1,0) wave-number implying no significant energy transfer to 2D higher harmonics, the amplification of oblique modes must be identified as the major contribution to this explosive growth of $(u_1')_{\max}$.

3.3 Case 3: Strongly Three-Dimensional Initial Conditions with Three-Dimensional Control

In this case, attention is focused on the applicability of three-dimensional control in the presence of a strongly three-dimensional initial field. In order to isolate the effects of interference with a 3D wave on an initially 3D vorticity field, no background disturbance was included. The initial disturbance field contained two and three-dimensional disturbances with $(u_1')_{2D}^{\max} = 0.03$ and $(u_1')_{3D}^{\max} = 0.01$ for each component. A 3D control wave (pulse) with peak amplitudes $0.025U_0$, $0.012U_0$, $0.006U_0$ was applied at $T=20$, $T=30$ and $T=40$, respectively; the controlled flow was then allowed to develop until $T=80$. The control wave contained all the 2D and 3D harmonics of the (u_2') -velocity at the channel center. In the laboratory, this would be equivalent to applying suction-blowing based on the u_2' -velocity at a position $(x_1=\text{const.}, x_2=0, x_3)$. The practical application of 3D control is, of course, a very difficult procedure but in this work we are mainly interested in the computational aspects and limits of the concept. A comparison of Figs. 6a and 6b indicates that, in the controlled flow, the amplitudes of $(u_1')_{\max}$, $(u_1')_{2D}$ -primary and its first four harmonics, as well as the amplitude of $(u_1')_{3D}$ -primary are all significantly reduced. After the application of the third control pulse at $T=40$, they all decay rapidly (Fig. 6b). Note that, in the uncontrolled flow, amplitudes of all the higher harmonics undergo rapid nonlinear growth and, when the 2D harmonics reach the level of the (1,0) mode, the flow goes through breakdown (Fig. 6a). A similar pattern can be observed in

the time-development of the maximum plane-averaged velocities and turbulent shear, the 3D control wave inhibits the growth of these quantities and, after $T > 40$, all the amplitudes decay rapidly.¹⁸ The "oscilloscope" traces of u_1' are shown in Fig. 7 at $T = 50$, wherein the uncontrolled wave presents three negative spikes characteristic of the final stage of transition indicating that the flow is rapidly approaching breakdown. Note that during the final stage of transition, the nonlinear distortions of the initially sinusoidal signal eventually degenerate into spikes caused by the slow moving fluid uplifted from the wall region due to the induced velocity of the counter-rotating streamwise vortices.¹⁵ The spanwise variations of $(u_1)_{\text{RMS}}^{\text{max}}$ in Fig. 8 reveal that the amplitudes are significantly reduced by the application of 3D control. However, the distribution remains in phase with the uncontrolled case.

The three-dimensional representations of vorticity components give perhaps the best display of the effectiveness of the control scheme.¹⁸ During transition, the streamwise vorticity (ω_x) field rapidly develops due to tilting of 2D spanwise vorticity (ω_z) and to stretching²⁰. The counterrotating vortex lobes strengthen by several orders of magnitude, in turn, causing greater spanwise variations in ω_z . This interaction evolves into a vortex loop extending towards the channel center. The uplifting and the consequent development of a high shear layer is one of the fundamental traits of transitional channel flow. Any effective control scheme must prevent this process. In Figs. 10a and 10b the isosurfaces of $\omega_z = 1.85$ at $T = 50$ are shown with and without control. In these figures, it can be depicted that in the uncontrolled case (Fig. 10a), the three-dimensional initial field has evolved into the characteristic vortex loop with evidence of flow breakdown. The controlled flow presents a contrasting development although the vorticity field at this stage does exhibit strong three-dimensional variations (Fig. 10b). It is clear from this figure that 3D control has prevented the uplifting and formation of the vortex loop and the associated high-shear layer. In the controlled flow, the spanwise structures completely disappear at later

times and the absence of any streamwise variations in the residual flow suggests that the flow may be locally laminarizing.¹⁸ Note that in laminar flow, a surface of constant ω_z would be a plane parallel to the wall. Similar traits can be observed from the development of the streamwise vorticity field¹⁸.

Finally, some results are presented from the temperature field that is treated as a passive scalar and used to tag the velocity/vorticity field. In Figs. 11a-11c, three-dimensional iso-temperature surfaces for $\theta=0.10$ are displayed. At $T=50$ the uncontrolled flow is characterized by vigorous mixing, resulting in a highly convoluted constant temperature surface, while the controlled flow remains more organized. The λ -vortices depicted at $T=50$ slowly decay, and finally at $T=80$, in accordance with the vorticity field, residual streamwise structures completely disappear lending evidence to local laminarization of the flow.

In order for this technique to be regarded as a potential candidate for flow control, various additional issues must also be considered. The "upstream influence" of the large-amplitude control pulse is one such question that is briefly addressed. Various plots of instantaneous streamwise velocity, u_1 , revealed that the effect of the control pulse manifests itself as a sharp kink very close to the wall which is rapidly dissipated by the action of viscosity with no residual effect on the flow development; similar smoothing action of strong viscous effects were observed in u_1 -RMS and $\langle u_1' u_2' \rangle$ -profiles in earlier work⁸. The second query of interest is a comparison of high-amplitude constant suction with the present method; a sample comparison is provided in Fig. 12. Here a constant suction velocity of $0.021 U_0$ (equal to the x_1 -averaged periodic suction velocity of case 3 at $T=20$) is imposed for one time step at $T=20$; the peak amplitude of the periodic control wave was $0.025 U_0$ for this case. As apparent from this figure, interference with periodic suction-blowing has a considerably more favorable effect on flow control than with constant suction for this strongly

three-dimensional disturbance field. However, this inference is for the three-dimensional case presented in this work and is not meant to be a general conclusion. Finally, a non-intrusive way of determining the control-wave phase from the surface pressure is proposed. For this purpose, a comparison of the respective control wave with surface pressure (at the same spanwise location) for 2D control (case 1) and 3D control (case 3) is presented. The relative phase angle of $\pi/2$ observed in Figs. 13 and 14 remains constant all through the flow development for both cases. Consequently, surface pressure signals could be used to determine the desired phase of the control pulse.

4. Concluding Remarks

In this computational study, the applicability of active control by periodic suction-blowing on transitional plane channel flow has been investigated. For two-dimensional finite-amplitude disturbances the method proved effective, reducing all the important Fourier amplitudes, turbulent intensities, and turbulent shear. In the presence of high-amplitude background noise, however, the gains derived from control were offset by the rapidly increasing oblique mode amplitudes which drive the flow to breakdown.

For strongly three-dimensional initial conditions with no background turbulence, three-dimensional control reversed the growth rates and significantly reduced disturbance amplitudes. By suppressing the streamwise vortex structure, the control wave prevented the formation of vortex loops, the development of the high shear-layer and the subsequent evolution to turbulent flow. The passive temperature field revealed the characteristics of the velocity/vorticity field with considerable accuracy.

The active control method studied in this work does show a potential for controlling disturbance growth rates in transitional flows with finite-amplitude disturbances. The feasibility of this concept and its usefulness as a viable tool

awaits careful comparisons with other existing techniques and experimental verification.

Acknowledgements

This work was supported by NASA/Langley Research Center under Contract NAG-1-462.

References

1. Harvey, W.D. and Pride, J.D., "The NASA/Langley LFC Airfoil Experiment", AIAA Paper 82-0567, 1982.
2. Milling, R.W., "Tollmien-Schlichting Wave Cancellation", Phys. Fluids, Vol 24, May 1981, pp. 201-204.
3. Thomas, A.S.W., "The Control of Boundary-Layer Transition Using a Wave-Superposition Principle," J. Fluid Mech., Vol 137, 1983, pp. 233-250.
4. Liepman, H.W., Brown, G.L. and Nosenchuck, D.M., "Control of Laminar Instability Waves Using a New Technique," J. Fluid Mech., Vol 118, 1982, pp. 187-200.
5. Gedney, C.J., "The Cancellation of Sound-Excited Tollmien-Schlichting Wave With Plate Vibration," Phys. Fluids, Vol. 26, May 1983, pp. 1158-1160.
6. Liepmann, H.W. and Nosenchuck, D.M., "Active Control of Laminar-Turbulent Transition," J. Fluid Mech., Vol. 118, 1982, pp. 201-204.
7. Bayliss, A., Maestrello, L., Parikh, P. and Turkel, E., "Numerical Simulation of Boundary Layer Excitation by Surface Heating/Cooling," AIAA Paper 85-0565, 1985.
8. Biringen, S., "Active Control of Transition by Periodic Suction-Blowing," Phys. Fluids, Vol. 27, May 1984, pp. 1345-1347.
9. Kleiser, L. and Laurien, E., "Numerical Investigation of Interactive Transition Control," AIAA Paper 85-0566, 1985.
10. Zang, T. and Hussaini, M.Y., "Numerical Experiments of Subcritical Transition Mechanisms, AIAA Paper 85-0286, 1985.
11. Metcalfe, R.W., Rutland, C., Duncan, J.H. and Riley, J.J., "Numerical Simulations of Active Stabilization of Laminary Boundary Layers," AIAA Paper 85-0567, 1985.
12. Kuhn, G.D., Moin, P., Kim, J. and Ferziger, J.H., "Turbulent Flow in a Channel With a Wall With Progressive Waves," Symposium on Laminar/Turbulent Boundary Layers, New Orleans, February 1984.
13. Strykowski, P.J. and Sreenivasan, K.R., "The Control of Transitional Flows," AIAA Paper 85-0559, 1985.
14. Moin, P., Reynolds, W.C. and Ferziger, J.H., "Large-Eddy Simulation of Incompressible Turbulent Channel Flow," Dept. Mech. Engrg., Stanford Univ., Rep. TF-11, 1978.
15. Biringen, S., "Final Stages of Transition to Turbulence in Plane Channel Flow," J. Fluid Mech., Vol. 148, 1984, pp. 413-442.
16. Biringen, S. and Maestrello, L., "Development of Spot-Like Turbulence in Plane Channel Flow," Phys. Fluids, Vol. 27, February 1984, pp. 318-321.
17. Herbert, M., "Secondary Instability of Plane Channel Flow to Subharmonic Three-Dimensional Disturbances," Phys. Fluids, Vol. 26, April 1983, pp. 871-874.

18. Biringen, S., Nutt, W.E. and Caruso, M.J., "Transition Control by Periodic Suction-Blowing", AIAA Paper 85-1700, 1985.
19. Nutt, W.E., "Transition Control and the Evolution of a Temperature Field in Plane Channel Flow", M.S. Thesis, Univ. of New Hampshire, September 1985.
20. Orszag, S.A. and Patera, A.T., "Secondary Instability of Wall-Bounded Shear Flows," J. Fluid Mech., Vol. 128, 1983, pp. 347-385.

TABLE I. Initial Conditionsⁱ

Case	α	β	u_{2D}^{\max}	u_{3D}^{\max}	u_{RAN}^{\max}	T_c ⁱⁱ	$(u_2)_c^{\max}$ ⁱⁱⁱ
1	1	1	3	0.5	0.01	20,30	2.3, 0.5
2	1	1	3	0.5	0.5	20	3.4
3	1	1	3	2	-	20,30,40	2.5,1.5,0.6

- (i) All velocities percent of U_0 ; (iii) $(u_2)_c$ is the control-wave peak amplitude.
(ii) T_c is time when control is applied

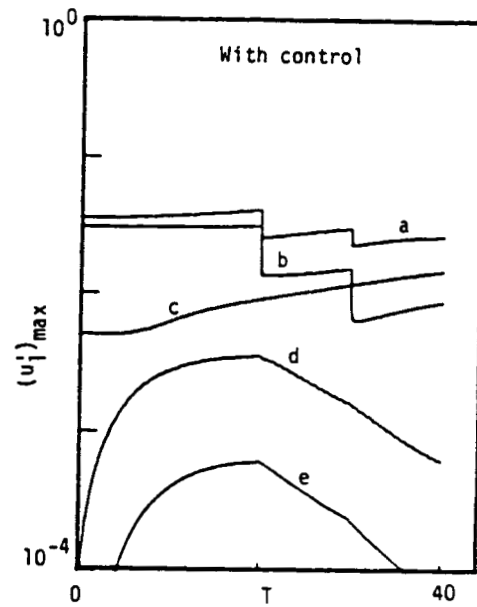
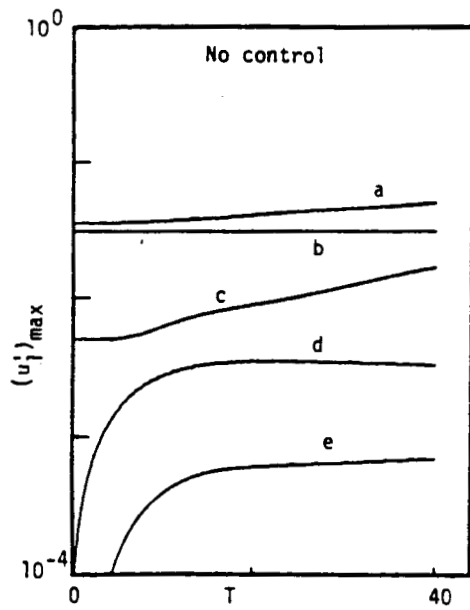


Figure 1. Temporal development of $(u_1')_{\max}$ for case 1. (a) Total, (b) 2D primary, (c) 3D primary, (d) 2D first harmonic, (e) 2D second harmonic.

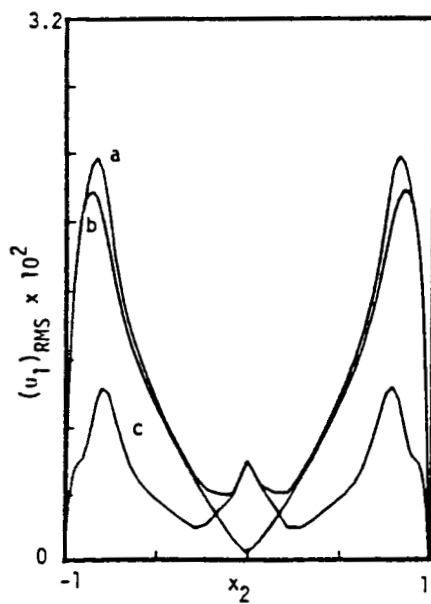


Figure 2. Distributions of the velocity correlations across the channel for case 1. (a) No control, $T=40$; (b) No control, $T=20$; (c) With control, $T=40$.

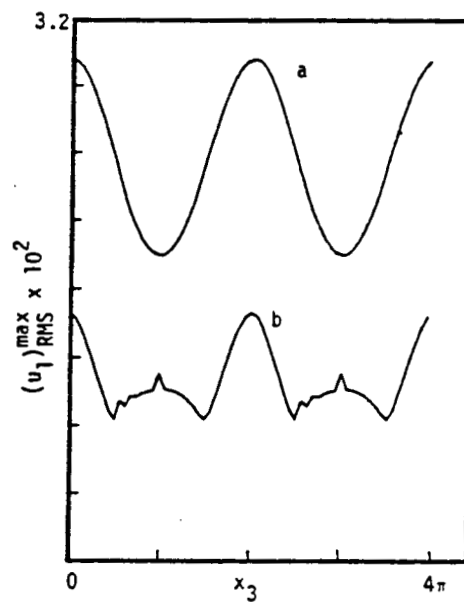


Figure 3. Spanwise variations of $(u_1')_{\text{RMS}}^{\max}$ for case 1 at $T=40$. (a) No control; (b) With control.

ORIGINAL PAGE IS
OF POOR QUALITY

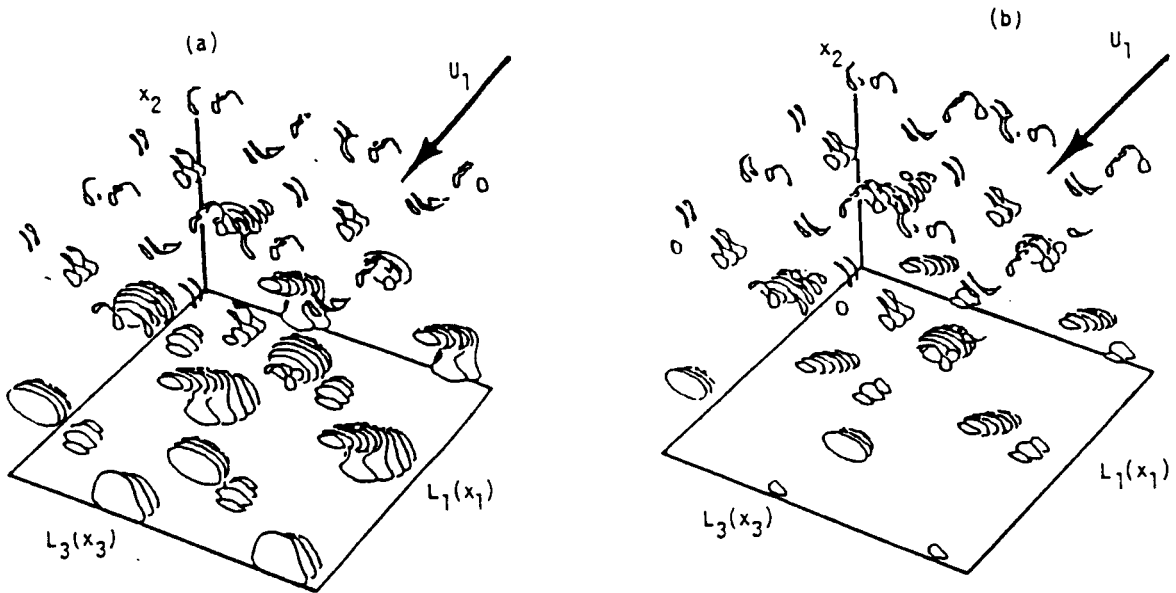


Figure 4. Iso-surfaces of streamwise vorticity, $w_x = 0.10$ for case 2 at $T = 40$; $0 \leq L_1 \leq 4\pi$, $\pi \leq L_3 \leq 5\pi$, $-1 \leq x_2 \leq 0$.
(a) No control; (b) With control.

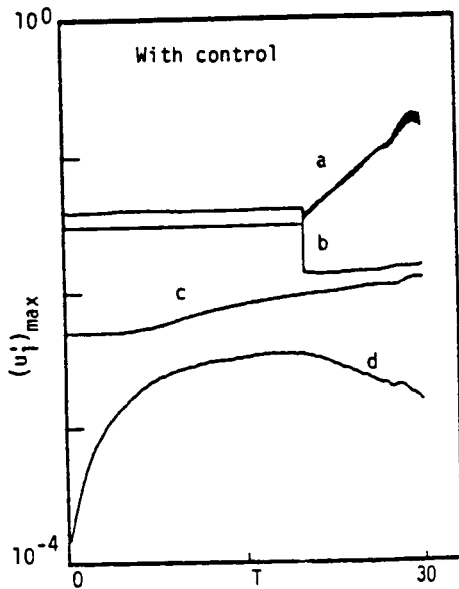


Figure 5. Temporal development of $(u_1)_{\max}$ for case 2. (a) Total, (b) 2D primary, (c) 3D primary, (d) 2D first harmonic.

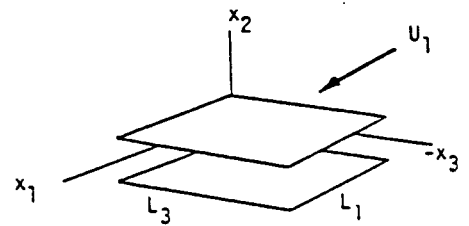


Figure 9. Coordinate frame for the iso-surface plots. $0 \leq L_1 \leq 4\pi$, $\pi \leq L_3 \leq 5\pi$, $-1 \leq x_2 \leq 0$.

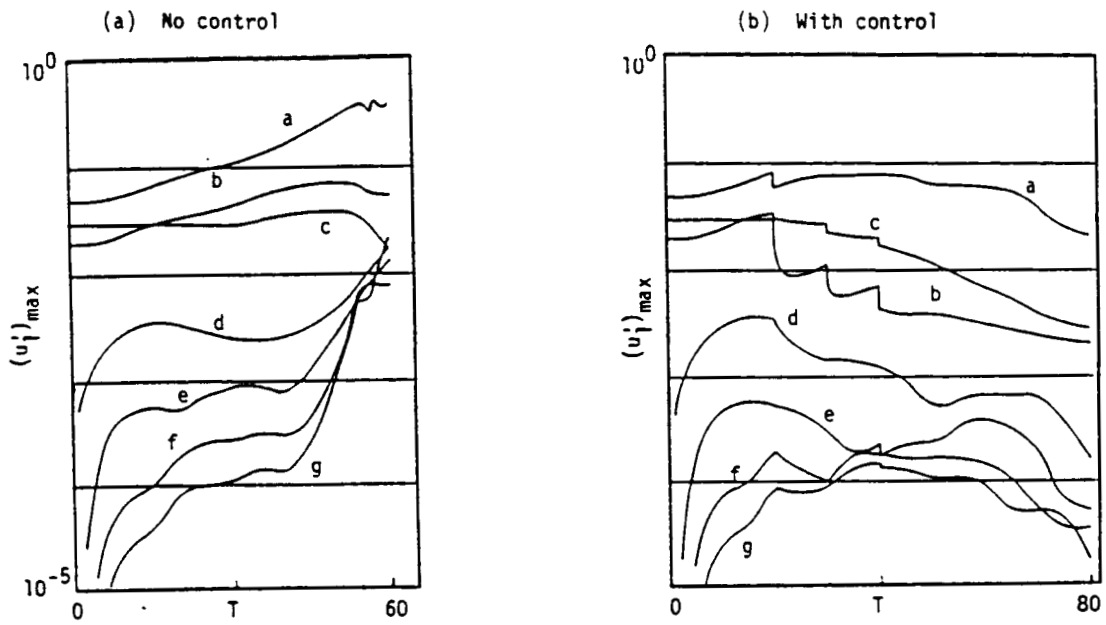


Figure 6. Temporal development of $(u_1')_{\max}$ for case 3. (a) Total, (b) 3D primary, (c) 2D primary, (d) 2D first harmonic, (e) 2D second harmonic, (f) 2D third harmonic, (g) 2D fourth harmonic.

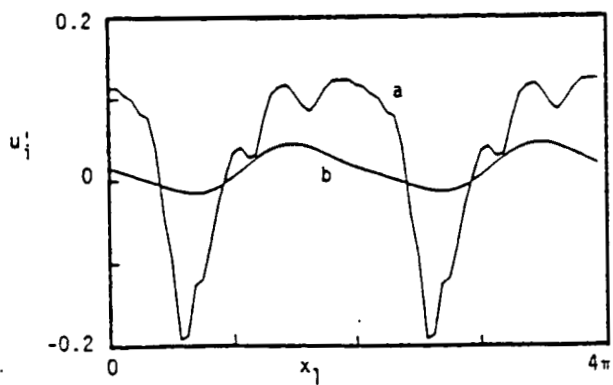


Figure 7. Fluctuations (at peak) of u_1' for case 3 at $T=50$. (a) No control; (b) With control.

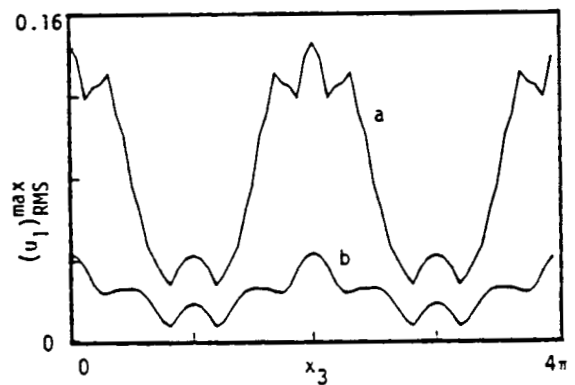


Figure 8. Spanwise variations of $(u_1')_{\text{RMS}}^{\max}$ for case 3 at $T=50$. (a) No control; (b) With control.

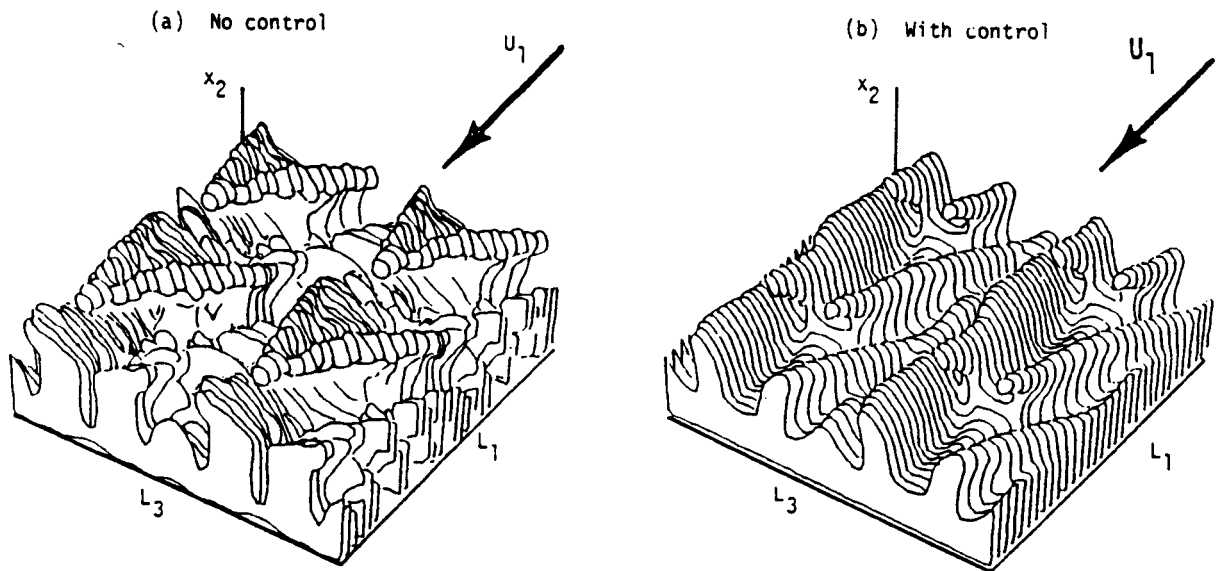
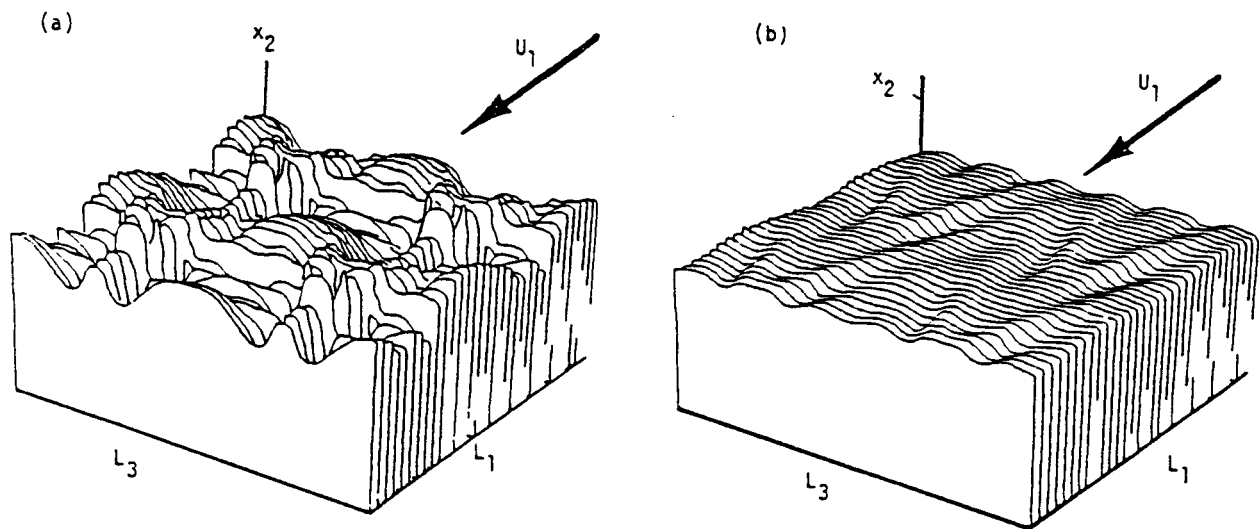


Figure 10. Isosurfaces of spanwise vorticity, $\omega_2 = 1.85$ for case 3 at $T=50$.



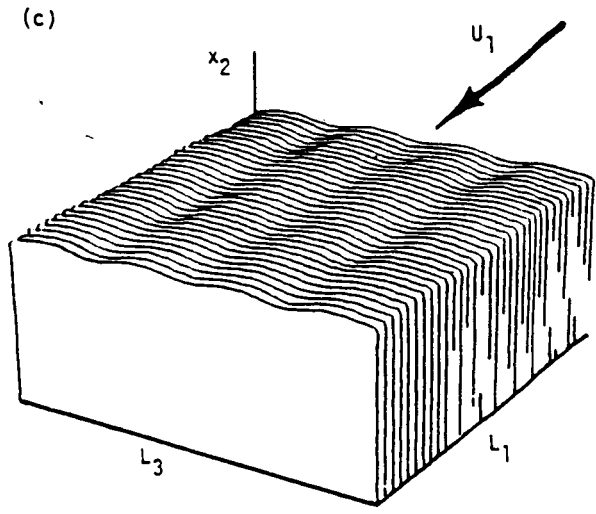


Figure 11. Isosurfaces of temperature, $\theta=0.1$ for case 3. (a) $T=50$, no control; (b) $T=50$, with control; (c) $T=80$, with control.

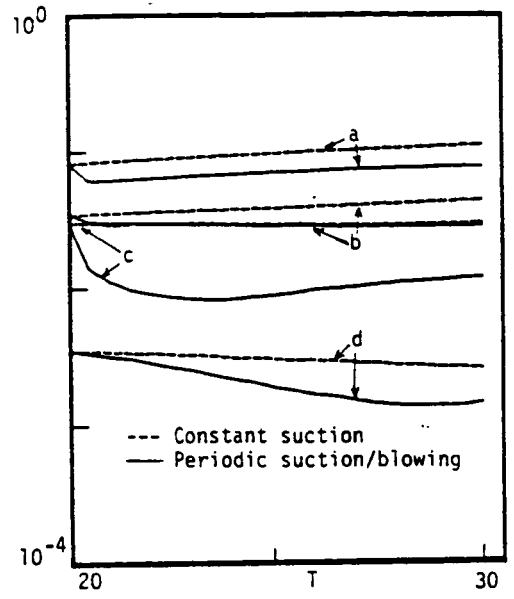


Figure 12. Temporal development of $(u_1')_{\max}$ for case 3, $20 \leq T \leq 30$. (a) Total, (b) 3D primary, (c) 2D primary, (d) 2D harmonic.

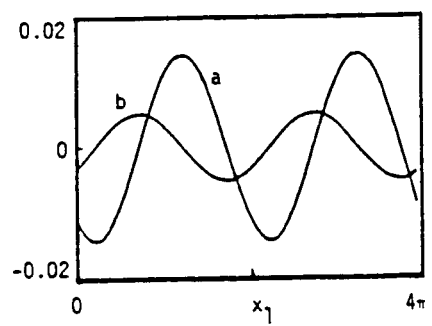


Figure 13. Comparison of 2D control wave (a) with surface pressure 2D component (b) for case 1 at $T=40$.

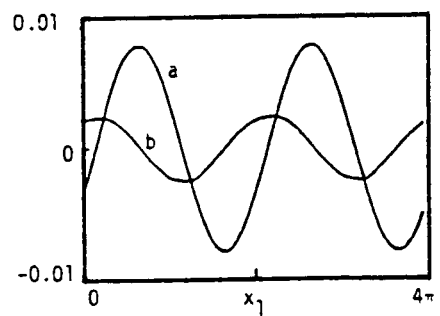


Figure 14. Comparison of 3D control wave (a) with surface pressure for case 3 at $T=30$.